A continuum based macroscopic unified low- and high cycle fatigue model

A continuum based macroscopic unified low- and high cycle fatigue model

Tero Frondelius[1,2,*], *Sami* Holopainen[3,**], *Reijo* Kouhia[3,***], *Niels Saabye* Ottosen[4,****], *Matti* Ristinmaa[4,†], and *Joona* Vaara[1,‡]

[1]Wärtsilä Finland Oy, Järvikatu 2-4, FI-65100 Vaasa, Finland
[2]Oulu University,
[3]Tampere University, P.O. Box 600, FI-33014 Tampere University, Finland
[4]Lund University, P.O. Box 117, SE-22100 Lund, Sweden

Abstract. In this work, an extension of a previously developed continuum based high-cycle fatigue model is enhanced to also capture the low-cycle fatigue regime, where significant plastic deformation of the bulk material takes place. Coupling of the LCF- and HCF-models is due to the damage evolution equation. The high-cycle part of the model is based on the concepts of a moving endurance surface in the stress space with an associated evolving isotropic damage variable. Damage evolution in the low-cycle part is determined via plastic deformations and endurance function. For the plastic behaviour a non-linear isotropic and kinematic hardening J2-plasticity model is adopted. Within this unified approach, there is no need for heuristic cycle-counting approaches since the model is formulated by means of evolution equations, i.e. incremental relations, and not changes per cycle. Moreover, the model is inherently multiaxial and treats the uniaxial and multiaxial stress histories in the same manner. Calibration of the model parameters is discussed and results from some test cases are shown.

1 Introduction

Fatigue dimension is the corner stone in engine building business [1]. Especially, in engine main components: crankshaft [2], connecting rod [3, 4] and cylinder head [5]. Ultrasonic fatigue testing [6] and Bayesian based statistical [7] fatigue testing have been a crucial step forward in understanding fatigue phenomena. In this paper, we focus a continuum based macroscopic combined low- and high-cycle fatigue model.

Fatigue of materials under variable loading histories is a complicated physical process which is characterized by nucleation, coalescence and stable growth of cracks. Nucleation of cracks starts from stress concentrations near persistent slip bands, grain boundaries and inclusions [8–10]. Depending on the intensity of loading two ranges of fatigue lives can be

*e-mail: tero.frondelius@wartsila.com,tero.frondelius@oulu.fi
**e-mail: sami.holopainen@tuni.fi
***e-mail: reijo.kouhia@tuni.fi
****e-mail: niels_saabye.ottosen@solid.lth.se
†e-mail: matti.ristinmaa@solid.lth.se
‡e-mail: joona.vaara@wartsila.com

classified, namely the low- and high-cycle regime. However, in recent years, it has been observed that fatigue failures can also occur at very high fatigue lives $10^9 - 10^{10}$, below the previously assumed fatigue limits for infinite life. In high-cycle fatigue, the macroscopic behavior of the material is primarily elastic, while in the low-cycle fatigue regime considerable macroscopic plastic deformations take place. Transition between low- and high-cycle fatigue for metallic materials occurs between $10^3 - 10^4$ cycles.

In this paper a unifield approach to model both low- and high-cycle fatigue of metals is proposed. The high-cycle fatigue part of the model is based on the concept of a moving endurance surface in the stress space with an associated evolving scalar damage variable. In this concept, originally proposed by Ottosen et al. [11] the movement of the endurance surface, as a function of the stress history, is tracked by an evolving back stress type of stress tensor. Therefore this model avoids the ambiguous cycle-counting techniques. It also facilitates consistent extensions to cope with anisotropic fatigue [12] as well as to include stress gradient effects [13], for alternative approaches see e.g. [14, 15]. Here, extension to handle also low-cycle fatigue is described. The low-cycle part of the model is formulated by a traditional nonlinear isotropic and kinematic hardening J2-plasticity model. The low and high cycle components are combined so that first, in case of yielding, the stress is returned onto the yield surface and then the damage is computed using a single damage evolution law. In case of elastic behaviour, the only contribution to the damage evolution is due to high-cycle fatigue model. The high-cycle fatigue damage is driven by the amount of violation of the endurance criterion while the low-cycle fatigue is driven in addition by the equivalent plastic strain.

2 Model formulation

2.1 High-cycle fatigue

An alternative approach to the popular critical plane approaches by Findley and Dang Van [16–18] was proposed by Ottosen et al. [11] which could be described as a continuum based approach. It is based on the assumption that a material exhibit "loading condition dependent endurance limits" within which no damage evolves under cyclic loading. These endurance limits are accomplished by defining a moving endurance surface in stress space. The second key ingedient of the continuum based fatigue model is adoption of the evolution laws which describe the movement of the endurance furface as well as damage evolution, which is defined in terms of stress increments and not in terms of stress cycles.

A function β that depends on the stress tensor and some internal variables is established and the endurance surface is then defined as

$$\beta(\boldsymbol{\sigma}, \{\boldsymbol{\alpha}\}; \text{parameters}) = 0, \tag{1}$$

where $\boldsymbol{\sigma}$ is the stress tensor and $\{\boldsymbol{\alpha}\}$ denotes the set of internal variables. Evolution of the internal variables and the damage are described by the evolution equations

$$\{\dot{\alpha}\} = \{\boldsymbol{G}\}(\boldsymbol{\sigma}, \{\boldsymbol{\alpha}\})\dot{\beta}, \qquad \text{and} \qquad \dot{D} = g(\beta, D)\dot{\beta}. \tag{2}$$

The form of the functions $\boldsymbol{G}$ and g are important for modelling the finite life durability, while the endurance surface determines the infinite life resistance. In contrast to rate-independent plasticity the stress state can lie outside the endurance surface and the evolution of the internal variables and the damage take place only when $\beta \geq 0$ and $\dot{\beta} > 0$.

In the original paper [11] the endurance surface is defined in a simple form

$$\beta = \frac{1}{\sigma_{-1}} (\bar{\sigma}_{\text{eff}} + AI_1 - \sigma_{-1}]) = 0, \tag{3}$$

where the reduced effective stress $\bar{\sigma}_{\text{eff}}$ is in the isotropic case defined in a usual way with the second invariant of the reduced deviatoric stress as

$$\bar{\sigma}_{\text{eff}} = \sqrt{3\bar{J}_2} = \sqrt{\tfrac{3}{2}(\boldsymbol{s}-\boldsymbol{\alpha}) : (\boldsymbol{s}-\boldsymbol{\alpha})} \tag{4}$$

in which $\boldsymbol{s}$ is the deviatoric stress tensor $\boldsymbol{s} = \boldsymbol{\sigma} - \frac{1}{3} I_1 \boldsymbol{I}$ and $I_1 = \operatorname{tr}\boldsymbol{\sigma}$. The endurance limit at zero mean stress is denoted as σ_{-1} instead of the usual expression $\sigma_{\text{af,R=-1}}$. The non-dimensional positive parameter A is the opposite value of the slope in the Haigh diagram and can be determined e.g. using formula $A = (\sigma_{-1}/\sigma_0) - 1$, where σ_0 is the fatigue limit amplitude for tensile pulsating loading ($R = 0$).

An alternative formulation utilizing the idea of [11] for the endurance surface was presented by Brighenti et al. [19] containing all the three stress invariants of the isotropy group.

A back stress like deviatoric tensor $\boldsymbol{\alpha}$, which memorizes the load history, is responsible for the movement of the endurance surface (3) in the stress space. It is illustrated in the deviatoric plane in Fig. 1 For the evolution of the α-tensor an evolution rule similar to Ziegler's

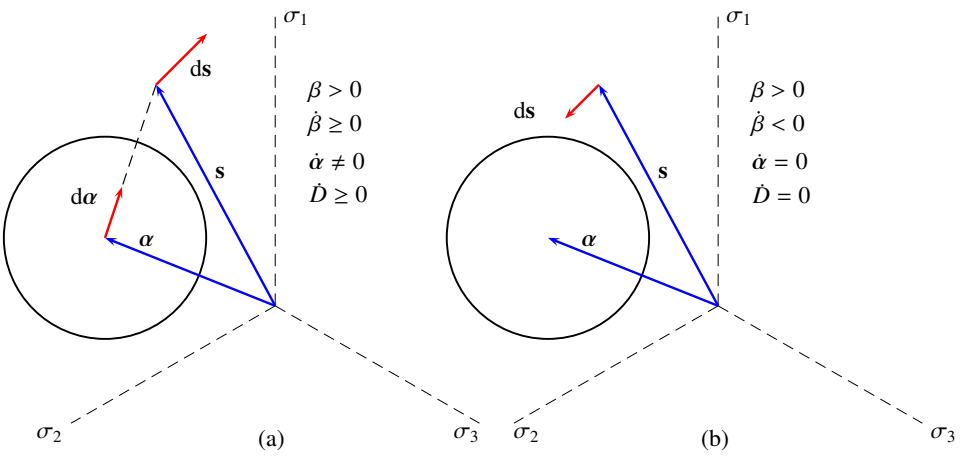

Figure 1. Illustration of damage evolution on the deviatoric plane. (a) Damage evolves only when stress moves away from the endurance surface. (b) Stress state outside the endurance surface, but damage do not evolve.

kinematic hardening rule in plasticity theory is adopted, i.e.

$$\dot{\boldsymbol{\alpha}} = C(\boldsymbol{s}-\boldsymbol{\alpha})\dot{\beta}, \tag{5}$$

where C is a non-dimensional material parameter, and the dot denotes time rate.

In the high-cycle range damage evolution can be successfully described by the following evolution equation

$$\dot{D} = g(\beta, D)\dot{\beta} = \frac{K}{(1-D)^k}\exp(L\beta)\dot{\beta}, \tag{6}$$

where K, L and k are dimensionless parameters. If $k = 0$ the damage increase per cycle will saturate to a constant value in a constant amplitude cyclic loading. However, in reality the

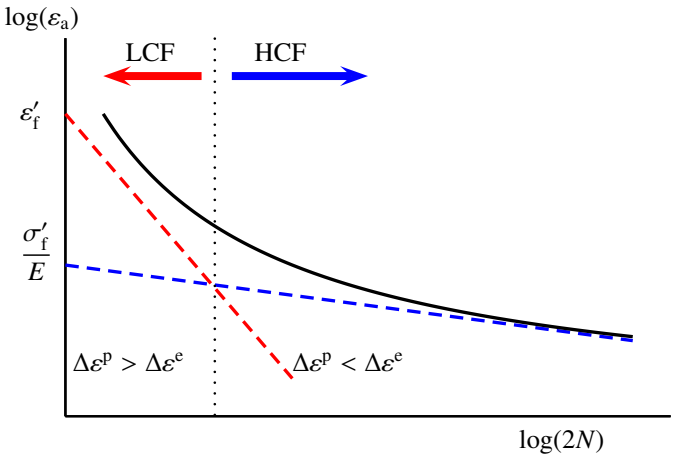

Figure 2. Strain-life diagram in double logarithmic scale.

damage rate increases with increasing damage and an alternative formulation with $k = 1$ is used in [12]. In that case, i.e. $k \geq 0$, damage rate per cycle increases with increasing damage, see the results in [20, Figures 6 and 7]. If $k \geq 1$ the order of loading sequence influences to the fatigue life which is an experimental observed phenomenon, however it makes estimation of parameters C, K and L more involved than in the case $k = 0$, see [12, Section 3].

2.2 Unified high- and low-cycle model

When performing the basic uniaxial fatigue test in the transition region between low-cycle and infinite life high-cycle fatigue, i.e. between $10^3 - 10^6$ cycles, combination of the Basquin and Manson & Coffin equations result in

$$\frac{1}{2}\Delta\varepsilon = \frac{\sigma'_f}{E}(2N)^{-b} + \varepsilon'_f(2N)^{-c}, \tag{7}$$

where σ'_f is the fatigue strength coefficient, b the fatigue strength exponent, ε'_f is the fatigue ductility coefficient and c is the fatigue ductility exponent. For metal materials the fatigue strength coefficient σ'_f is close to the true tensile rupture stress of a material and the ductility coefficient is close to rupture strain. The numerical values of the fatigue strength exponent is usually between $0.05 - 0.12$ and the ductility exponent between $0.5 - 0.7$. Relation (7) are schematically illustrated in Fig. 2. Tabulated values of $\sigma'_f, \varepsilon'_f, b$ and c for different materials can be found in the literature, e.g. [21].

In the LCF-region the HCF-model described in section 2.1 has to be coupled to the elasto-plastic constitutive model. As in the original formulation by Ottosen et al. [11] a scalar damage variable is chosen to descibe the material deterioration due to fatigue. In the unified LCF-HCF-model the chosen evolution equation for the damage D is

$$\dot{D} = \phi(\xi)g(\beta, D)\dot{\beta} + (1 - \phi(\xi))\hat{g}(\varepsilon^p_{\text{eff}}, \dot{\varepsilon}^p_{\text{eff}}, \varepsilon_{\text{eff}}, \dot{\varepsilon}_{\text{eff}}, \beta, \dot{\beta}), \tag{8}$$

where $\phi(\xi)$ is the logistic function

$$\phi(\xi) = \frac{1}{1 + \exp((\xi - \xi_0)/s)}, \quad \xi = \frac{\dot{\varepsilon}^p_{\text{eff}}}{\dot{\varepsilon}_{\text{eff}}}, \tag{9}$$

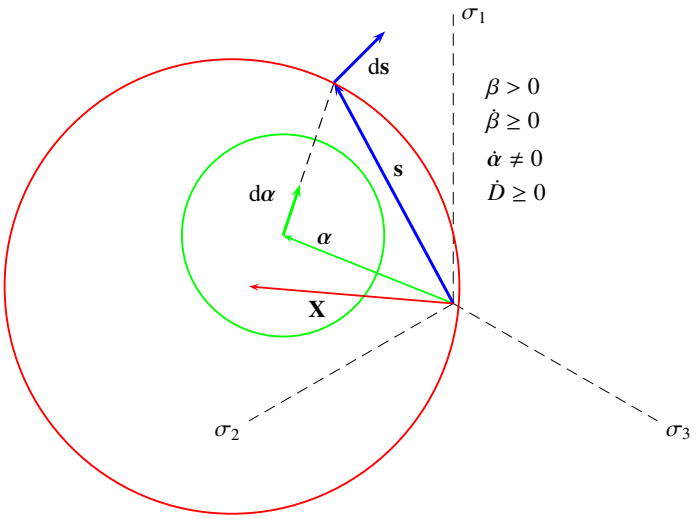

Figure 3. Illustration of the unifield fatigue model in the deviatoric stress space.

and the low cycle part $\hat{g}$ is

$$\hat{g}(\varepsilon^{\mathrm{p}}_{\mathrm{eff}}, \dot{\varepsilon}^{\mathrm{p}}_{\mathrm{eff}}, \varepsilon_{\mathrm{eff}}, \dot{\varepsilon}_{\mathrm{eff}}, \beta, \dot{\beta}) = M \frac{\mathrm{d}}{\mathrm{d}t} \left\{ \left[\frac{\varepsilon^{\mathrm{p}}_{\mathrm{eff}}}{\varepsilon_{\mathrm{eff}}} \exp(L\beta) \right]^m \right\}, \tag{10}$$

where M, m, s, ξ_0 are additional material parameters and $\varepsilon^{\mathrm{p}}_{\mathrm{eff}}$ is the effective plastic strain defined as usual

$$\varepsilon^{\mathrm{p}}_{\mathrm{eff}} = \int \dot{\varepsilon}^{\mathrm{p}}_{\mathrm{eff}} \, \mathrm{d}t, \quad \dot{\varepsilon}^{\mathrm{p}}_{\mathrm{eff}} = \sqrt{\tfrac{2}{3} \dot{\boldsymbol{\varepsilon}}^{\mathrm{p}} : \dot{\boldsymbol{\varepsilon}}^{\mathrm{p}}}. \tag{11}$$

The effective strain $\varepsilon_{\mathrm{eff}}$ is defined analogously. A natural value for the parameter ξ_0 is 0.5 since it just indicates the transition between the low-and high cycle fatigue, see Fig. 2. Moreover, it is obvious that m is approximately the reciprocal of the ductility exponent c in the strain-life equation (7).

There are myriad of different non-linear isotropic-kinematic hardening plasticity models available, see e.g. [22, 23] In this study Chaboche-type J_2-plasticity model is adopted for which the yield function and the evolution equations are [24–26]

$$f(\boldsymbol{\sigma}, \boldsymbol{X}, R) = \sqrt{\tfrac{3}{2}(\boldsymbol{s} - \boldsymbol{X}) : (\boldsymbol{s} - \boldsymbol{X})} - (\sigma_{\mathrm{y}} + R) = 0, \tag{12}$$

$$\dot{R}_i = \gamma R_{\infty,i} \left(1 - R_i / R_{\infty,i}\right) \dot{\varepsilon}^{\mathrm{p}}_{\mathrm{eff}}, \qquad R = \sum R_i, \tag{13}$$

$$\dot{\boldsymbol{X}}_i = \tfrac{2}{3} X_{\infty,i} \dot{\boldsymbol{\varepsilon}}_{\mathrm{p}} - \gamma_i \dot{\varepsilon}^{\mathrm{p}}_{\mathrm{eff}} \boldsymbol{X}_i, \qquad \boldsymbol{X} = \sum \boldsymbol{X}_i, \qquad \dot{\boldsymbol{\varepsilon}}_{\mathrm{p}} = \dot{\lambda} \frac{\partial f}{\partial \boldsymbol{\sigma}}. \tag{14}$$

where $\boldsymbol{X}$ is the back-stress defining the center of the yield surface, see Fig. 3.

3 Examples

3.1 Computation of SN-curve

As an example the SN-curve of the annealed AISI 4340 steel with ultimate tensile strength of 827 MPa has been computed. The material parameters in the fatigue damage model are:

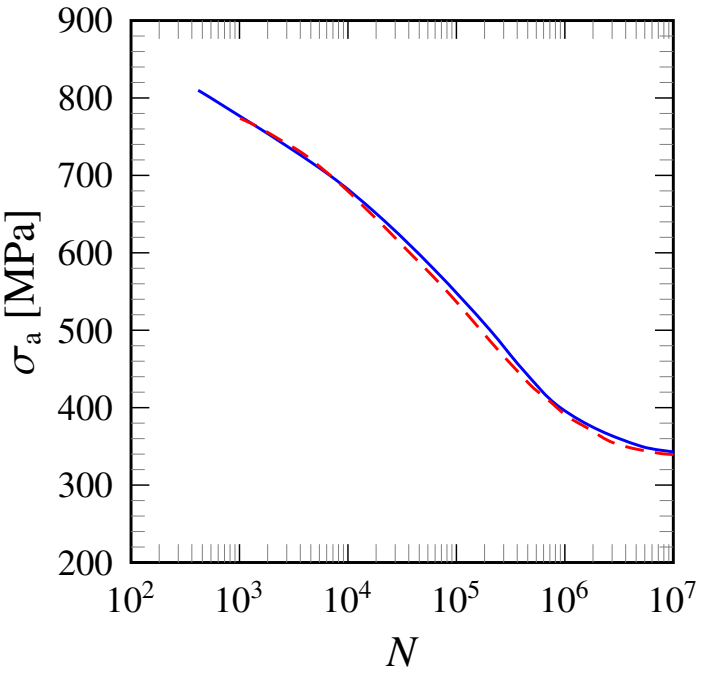

Figure 4. SN fatigue life curve for the AISI 4340 steel. Model results are shown with solid blue line and the fit to experimental data [27] with dashed red line.

σ_{-1} = 315 MPa, A = 0.225, C = 1.0, $K = 3.5 \cdot 10^{-6}$, L = 7, $M = 2 \cdot 10^{-8}$, ξ_0 = 0.5, m = 1.6, and s = 0.1. Moreover, for the nonlinear kinematic hardening model the following parameters are used: σ_y = 331 MPa, $X_{\infty,1}$ = 35912 MPa, $X_{\infty,2}$ = 6972 MPa, $X_{\infty,3}$ = 4222 MPa, γ_1 = 651, γ_2 = 53.3 and γ_3 = 5.7 [27]. Comparison to the SN-curve based on fitting the experimental data in [27] is shown Fig. 4.

3.2 Two-level test simulation

Fig. 5 shows the model predictions together with experimantal data under a two-level loading ($R = -1$). The grade of the AISI 4340 steel used in the calibration shown in [27, Fig. 3] slightly differs from that used in the experiments for the two-level loadings, cf. [28, Table II]. A consequence is that the fatigue lives of steel that has been applied for the experimentation in the two-step loadings are considerably longer: $N(\sigma = 735\,\text{MPa})/N(\sigma = 810\,\text{MPa}) = 2860/420 = 6.8$ by the model, whereas $N(\sigma = 735\,\text{MPa})/N(\sigma = 810\,\text{MPa}) = 83800/37100 = 2.3$ by the steel in [28].

4 Concluding remarks

A unified low- and high-cycle fatigue model based on continuum mechanics is developed. Coupling of the LCF- and HCF-models is due to the damage evolution equation. The high-cycle part of the model is based on the concepts of a moving endurance surface in the stress space, while the damage evolution in the low-cycle part of the model is also due to plastic deformations. Adopted plasticity model is based on the classical J2-plasticity model with

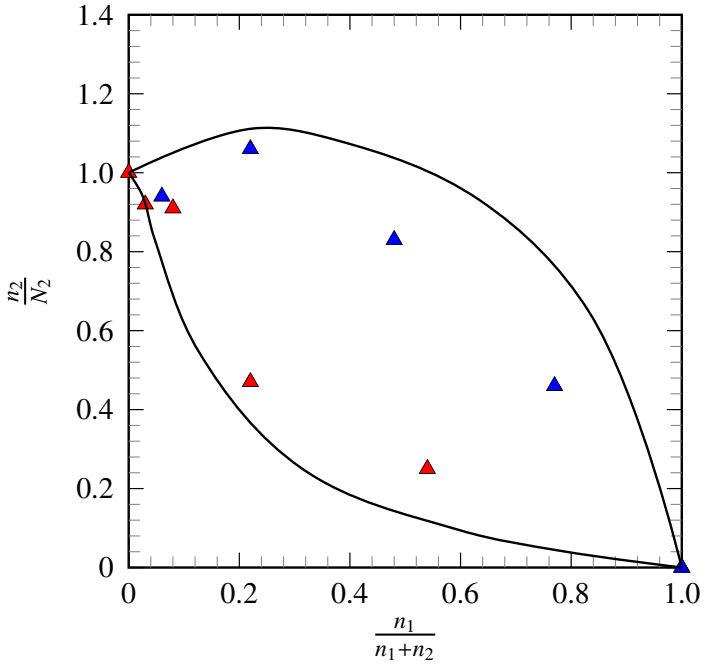

Figure 5. Comparison of model predictions (solid lines) to the experimental results which are demonstrated by triangles, [28, Fig. 4], for two-level loadings when the stress ratios are 810 MPa/735 MPa=1.10. The lower (red color) and upper (blue color) markers implicate the loadings from high to low and low to high, respectively. In the model predictions the properties of the AISI 4340 steel are used.

nonlinear Chaboche type isotropic and kinematic hardening. As an example, the model parameters have been fitted to the SN-data for the AISI 4340 steel. Further research is focused in relating the fatigue model parameters to the standard Basquin-Coffin-Manson parameters, which are available in literature for most materials. Moreover, the model should be verified against more complex loading sequences. However, such test data is scarse in the literature.

Acknowledgements.

This research has been supported in part by Business Finland (former Tekes - the National Technology Agency of Finland), project MaNuMiES, project 3361/31/2015 and WIMMA 1566/31/2015.

References

[1] T. Frondelius, H. Tienhaara, M. Haataja, Rakenteiden Mekaniikka **51**, 1 (2018)
[2] I. Väisänen, A. Mäntylä, A. Korpela, T. Kuivaniemi, T. Frondelius, Rakenteiden Mekaniikka **50**, 341 (2017)
[3] J. Göös, A. Leppänen, A. Mäntylä, T. Frondelius, Rakenteiden Mekaniikka **50**, 275 (2017)
[4] A. Mäntylä, J. Göös, A. Leppänen, T. Frondelius, Rakenteiden Mekaniikka **50**, 239 (2017)

[5] A. Leppänen, A. Kumpula, J. Vaara, M. Cattarinussi, J. Könnö, T. Frondelius, Rakenteiden Mekaniikka **50**, 182 (2017)
[6] J. Korhonen, J. Kuoppala, M. Väntänen, J. Vaara, M. Turunen, P. Kämäräinen, J. Laine, A. Silvonen, T. Frondelius, Rakenteiden Mekaniikka **50**, 304 (2017)
[7] M. Väntänen, J. Vaara, J. Aho, J. Kemppainen, T. Frondelius, Rakenteiden Mekaniikka **50**, 201 (2017)
[8] S. Suresh, *Fatigue of Materials*, 2nd edn. (Cambridge University Press, 1998)
[9] V. Bolotin, *Mechanics of Fatigue*, CRC Mechanical Engineering Series (CRC Press, Boca Raton, 1999)
[10] D. Socie, G. Marquis, *Multiaxial Fatigue* (Society of Automotive Engineers, Inc., Warrendale, Pa, 2000)
[11] N. Ottosen, R. Stenström, M. Ristinmaa, International Journal of Fatigue **30**, 996 (2008)
[12] S. Holopainen, R. Kouhia, T. Saksala, European Journal of Mechanics A/Solids **60**, 183 (2016)
[13] N. Ottosen, M. Ristinmaa, R. Kouhia, International Journal of Fatigue **116**, 128 (2018)
[14] F. Morel, T. Palin-Luc, Fatigue & Fracture of Engineering Materials & Structures **25**, 649 (2002)
[15] D. Luu, M. Maitournam, Q. Nguyen, International Journal of Fatigue **61**, 170 (2014)
[16] W. Findley, Journal of Engineering for Industry pp. 301–306 (1959)
[17] K. Dang Van, G. Cailletaud, G. Flavenot, A. Le Douaron, H. Lieurade, *Criterion for high cycle fatigue failure under multiaxial loading*, in *Biaxial and Multiaxial Fatigue*, edited by M. Brown, K. Miller (Mechanical Engineering Publications, London, 1989), Number 3 in EGF, pp. 459–478
[18] J. Vaara, A. Mäntylä, T. Frondelius, Rakenteiden Mekaniikka **50**, 146 (2017)
[19] R. Brighenti, A. Carpinteri, S. Vantadori, Fatigue & Fracture of Engineering Materials & Structures **35**, 141 (2012)
[20] S. Holopainen, R. Kouhia, J. Könnö, T. Saksala, Procedia Structural Integrity **2**, 2718 (2016)
[21] AMS, *Metals Handbook*, Vol. 1, 9th edn. (Properties and Selection: Irons and Steels, Metals Park OH, 1978)
[22] J. Lemaitre, J.L. Chaboche, *Mechanics of Solid Materials* (Cambridge University Press, 1990)
[23] N. Ottosen, M. Ristinmaa, *The Mechanics of Constitutive Modeling* (Elsevier, 2005)
[24] A. Benallal, R. Billardon, J. Lemaitre, in *Fracture 84*, edited by S. Valluri, D. Taplin, P.R. Rao, J. Knott, R. Dubey (Pergamon, 1984), pp. 3669 – 3676
[25] J. Lemaitre, Computer Methods in Applied Mechanics and Engineering **51**, 31 (1985)
[26] J. Chaboche, International Journal of Plasticity **24**, 1642 (2008), special Issue in Honor of Jean-Louis Chaboche
[27] Y. Gorash, D. MacKenzie, Open Engineering **7**, 126 (2017)
[28] W. Erickson, C. Work, *A study of the accumulatiob of fatigue damage in steel*, in *64th Annual Meeting of ASTM* (1961), pp. 704–718